Direct noise computation of a shocked and heated jet at a Mach number of 3.30

Nicolas de Cacqueray* , **Christophe Bogey†** and **Christophe Bailly‡**

Laboratoire de Mécanique des Fluides et d'Acoustique

UMR CNRS 5509, Ecole Centrale de Lyon

69134 Ecully, France

An overexpanded axisymmetric jet at an exit Mach number of 3.30 and a Reynolds number of 10^5 is computed by compressible large-eddy simulation (LES) to determine directly its radiated sound field, using low-dissipation schemes in combination with an adaptative shock-capturing method. At the jet nozzle exit, static pressure and temperature are respectively equal to 0.5×10^5 Pa and 360 K, and a laminar flow profile is imposed. To assess the validity of the simulation, the mean aerodynamic field and the near-field pressure levels, obtained directly by LES, are compared to available literature data. The axial velocity fluctuations in the shear-layer are also characterized using azimuthal decomposition, and exhibit properties close to those observed in screeching jets. The acoustic field is dominated by axisymmetric and first azimuthal modes, and noise sources are investigated from the acoustic near field: Mach waves, shock-associated noise and turbulent mixing noise occuring around the end of the potential core are identified.

I. Introduction

Propulsive jets of space launchers are highly supersonic with an equivalent fully expanded Mach number M_j higher than 2, heated and not perfectly expanded. They are also known to generate a strong acoustic field, which might induce vibrations during the lift-off. Unfortunately, there is a little number of experimental[1–4] and computational[5,6] studies on this kind of jets, and it is usually assumed that Mach waves are the dominant noise generation mechanism.[7–10]

In high-Reynolds-number subsonic jets, two noise components have been identified.[11–14] One is dominating in the downstream direction with a noise source located around the end of the potential core,[15,16] and another is dominating in the sideline direction and is probably linked with the turbulent mixing in the shear layer.[12,16] The continuity of the acoustic spectra between subsonic and supersonic jets has been shown by Tam *et al.*,[11] which suggests that noise components are similar. In addition to subsonic jet noise components, specific noise sources can however be found in supersonic jets such as Mach waves and shock-associated noise. Mach waves indeed occur when the convection velocity of turbulent structures is supersonic.[17] They are highly directive, and have a plane wave-like geometry in the acoustic near field. Other sound sources are associated with the fact that supersonic jets are usually characterized by static pressure at the nozzle exit strongly different from that of the ambient field. This variation of static pressure leads to the presence of a shock-cell structure in the jet plume. The interactions between turbulent structures and shock cells thus generate broadband noise[18,19] propagating both in the upstream and downstream directions.[18,20] If the jet shear layer at the nozzle exit is sufficiently receptive to the upstream propagating acoustic excitation,[21–23] a feedback loop can also occur, and generate a tonal noise called *screech*, first observed by Powell[24] in the 1950s. The screech tone radiates mainly in the upstream direction, and Tam & *al.*,[22] for instance, have shown that the screech fundamental frequency and the central frequency of the broadband shock-associated noise collapse in the upstream direction. In a screeching jet, the whole jet in addition oscillates at the fundamental and harmonic screech frequencies.[21,25,26]

*PhD student, nicolas.cacqueray@ec-lyon.fr

†CNRS Research Scientist, AIAA Member, christophe.bogey@ec-lyon.fr

‡Professor at Ecole Centrale de Lyon & Institut Universitaire de France, Senior AIAA Member, christophe.bailly@ec-lyon.fr

Most of experimental studies on supersonic jets with an exit Mach number higher than 2 have been carried out for adapted jets[1,3,4,9] which should naturally not contain shock cell. In such jets, Mach waves radiated by linear instability waves are assumed to be the dominant noise component.[7–9] Based on this, early numerical studies on propulsive jets have been performed in the nineties for fully-expanded jets by solving linear Euler equations.[27] With the increase of computational resources, three-dimensionnal Navier-Stokes simulations is however now possible for propulsive jets.[28] Results from non-linear computations and linear stability theory have for instance been compared by Mohseni *et al.*[29] and Ryu *et al.*[30] These authors have found a limited agreement for large turbulent scales and for the radiated acoustic field, thus suggesting that the non-linear behaviour of the turbulence play an important role for Mach wave radiation. Unfortunately, very few experimental[2,31] and numerical[5] studies exist on shocked propulsive jets. Therefore, the influence of the shock-cell structure on turbulence and on Mach wave generation is not well established yet.

Over the past ten years, the development of low-dissipation and low-dispersion numerical schemes[32–34] has permitted to carry out direct noise computation (DNC) for turbulent flows. The implementation of a shock-capturing method is also necessary in supersonic flows to remove Gibbs oscillations near shocks.[35] However, a particular attention must be paid to the possible artificial dissipation of the turbulent structures and shocks motion[35] by the shock capturing procedure. Over the last years, DNC has been successfully applied to high-Reynolds-number subsonic jets to study noise sources[16] using large-eddy simulation (LES) approach.[36,37] Several DNC using LES have also been performed for supersonic jets,[21,38–40] but only few computations have been done on shocked propulsive jets.[5]

In the present study, DNC is applied to a shocked propulsive jet with an exit Mach number of 3.30 and stagnation temperature and pressure of 1144 K and 28.6×10^5 Pa in order to show the feasibility of using this approach for propulsive jets, and to give a first insight into noise sources. The jet exit conditions are similar to those inthe experiment of Varnier & Gély.[31] The computation of the flow and of the radiated sound fields is performed using compressible large-eddy simulation. The axial velocity fluctuations along the shear layer and the near acoustic field pressure are characterized using spectral analysis and azimuthal decomposition. To identify noise sources, the connections between the turbulent flow and the acoustic field are tracked.

The outline of the paper is the following. In the first section, the numerical procedure and the simulation parameters are presented. In the second section, snapshots of vorticity, of numerical schlieren pictures, and of fluctuating pressure are shown. Then, in the third section, the mean aerodynamic field is examined, and the properties of shear layer velocity fluctuations are explored according to their azimuthal components. Finally, near-field and far-field acoustic results are presented and a noise source identification is performed on the acoustic near-field from the links exhibited with the turbulent flow, and for the comparison with experimental, numerical and theoritical works.

II. Numerical procedure

A. Simulation parameters

In the present work, an overexpanded jet at an exit Mach number of $M_e = 3.30$, an exit temperature of $T_e = 360$ K and an exit static pressure of $p_e = 0.5 \times 10^5$ Pa, originating at $z = 0$ from a pipe nozzle of length $0.5r_e$ where r_e is the nozzle radius, is considered. The stagnation pressure p_0 and temperature T_0 are respectively 28.6×10^5 Pa and 1144 K. The equivalent fully expanded conditions defined from the same stagnation conditions and a static pressure of $p_j = 10^5$ Pa are a Mach number of $M_j = 2.83$, a temperature of $T_j = 439$ K and a radius of $r_j = 0.81r_e$. The acoustic Mach number M_a defined as the ratio of the fully expanded velocity u_j over the ambient sound speed c_∞ is equal to 3.47. The Reynolds number Re estimated from the exit quantities is equal to 0.94×10^5. At the inlet, a Blasius profile for a laminar boundary layer of thickness $\delta = 0.05r_e$ is imposed for the mean velocity and a Crocco-Busemann profile is used for the mean density. Random pressure disturbances of low amplitude are introduced in the nozzle, yielding nozzle-exit maximum velocity fluctuations of 0.3% of the jet exit velocity.

The jet exit quantities are similar to those of an experiment performed at LEA Poitiers on MARTEL facility.[31] However, due to numerical limitations, the Reynolds number of the simulation is 20 times smaller than the Reynolds number of the experiment. Jet exit parameters of the present computation and of the experiment carried out on MARTEL facility[31] are given in table 1.

	M_e	p_e	T_e	Re
Present computation	3.30	0.50×10^5 Pa	360° K	0.94×10^5
Experiment[31]	3.27	0.51×10^5 Pa	359° K	17.5×10^5

Table 1. Jet exit parameters: Mach number M_e, static pressure p_e, temperature T_e and Reynolds number Re.

B. Numerical methods

The simulation is performed by solving the unsteady compressible Navier-Stokes equations in cylindrical coordinates, using low-dispersion and low-dissipation finite-difference schemes:[34,35,41] 11 points 4^{th}-order finite differences and 6^{th}-order filter for space discretization, and 2^{nd}-order 6-stage Runge-Kutta algorithm for time integration. For the treatment of the axis singularity, the method proposed by Mohseni & Colonius[42] is used, and to increase the time step, the effective azimuthal resolution is reduced near the jet centerline.[43] The LES approach is based on the explicit application of a relaxation filtering to the flow variables[37] to take into account the dissipative effects of the subgrid scales. Non-reflective acoustic boundary conditions[44] are implemented for radial and upstream boundaries. A sponge zone is used in the downstream direction to minimize acoustical reflections at the outflow boundary.[44] Similar numerical methods have been successfully implemented in previous LES of subsonic round jets[16,45] and of a supersonic plane jet.[21] An adaptative and conservative shock-capturing method is here used to remove Gibbs oscillations near shocks.[35]

The grid used for the present jet contains $n_r \times n_\theta \times n_z = 256 \times 128 \times 840 = 28 \times 10^6$ points, and 120,000 iterations carried out using NEC SX - 8 computers have been necessary to ensure statistical convergence. The radial and the axial mesh spacings are presented in figure 1. In the radial direction, the mesh is refined down to $\Delta r_{nozzle} = 0.0072 r_e$ at the nozzle lip to properly solve the shear layer, and it is then stretched up to $\Delta r_{acou} = 0.1 r_e$. Near the radial boundaries, the mesh is stretched again in order to apply non-reflective acoustic boundary conditions based on far-field approximations.[44] In the axial direction, the mesh size is constant in the nozzle and equal to $\Delta z_{nozzle} = 4\Delta r_{nozzle}$, then the mesh is stretched up to $\Delta z_{acou} = 0.074 r_e$. Finally, the sponge zone is built by increasing the axial mesh size.

To compute far-field noise spectra and directivities, the LES near-field obtained on a control surface located at $r = 9.5 r_e$ is propagated to 50 radii from the nozzle exit, by solving the full Euler equations with the shock-capturing procedure[35] on a constant grid of $561 \times 128 \times 1001 = 72 \times 10^6$ points. The mesh spacing for acoustic propagation is equal to $\Delta r_{acou} = 0.1 r_e$ in the radial direction, and to $\Delta z_{acou} = 0.074 r_e$ in the axial direction. The numerical cut-off Strouhal number for acoustic propagation is thus $St_c = 2 f_c r_e / u_e = 1.37$ where $f_c = c_\infty / (4\Delta r_{acou})$ and u_e is the jet exit velocity equal to 1255 m/s.

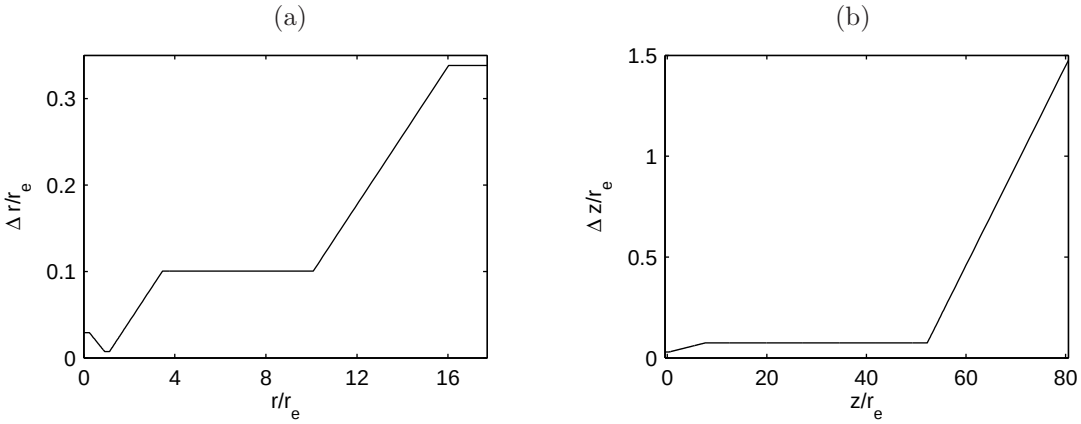

Figure 1. Mesh sizes, Δr and Δz, of the grid in the LES computation respectively in (a) the radial and in (b) the axial directions.

(a)

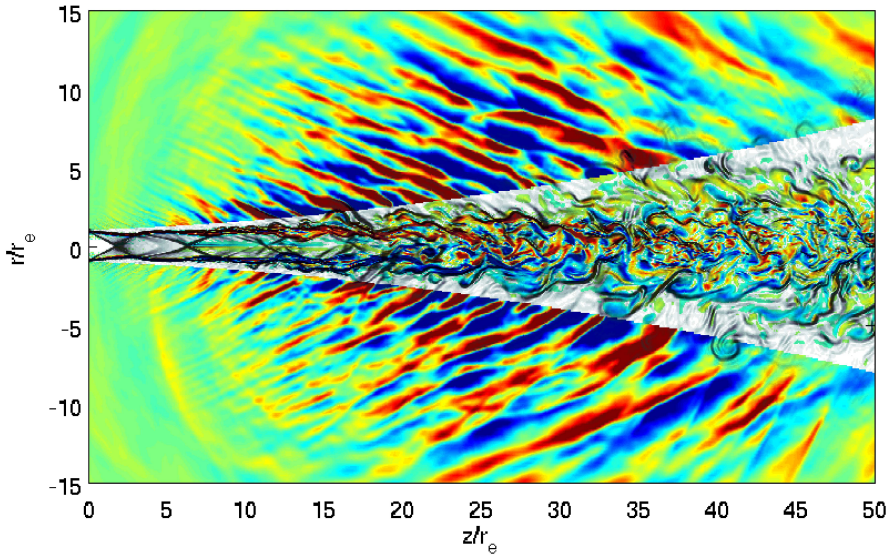

(b)

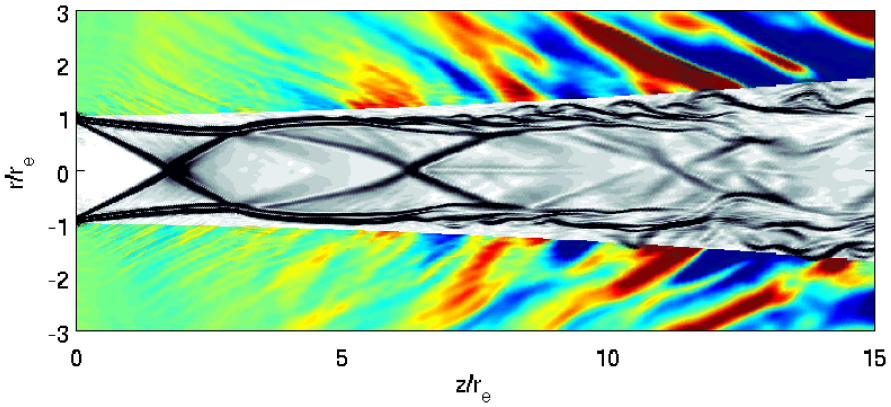

Figure 2. Snapshots in the (z, r) plane of the present simulation: (a) density gradient norm $\nabla\rho$ in gray scale, azimuthal vorticity ω_θ in color scale in the jet and fluctuating pressure p' in color scale outside the jet, and (b) density gradient norm $\nabla\rho$ in gray scale and fluctuating pressure p' in color scale outside the jet. The color scale ranges for levels from -5000 to 5000 Pa for p'.

III. Instantaneous fields

Snapshots of azimuthal vorticity ω_θ, of density gradient norm $\nabla\rho$ and of fluctuating pressure are shown in figure 2 (a). The distances are made dimensionless with respect to the nozzle radius r_e. Shock-cells and temperature fronts are visible from the density gradient field. The development of the turbulence along the shear layers and turbulent mixing are observed. Moreover, vorticity generated from shock interactions[46] close to the jet centerline is also noticed in the potential core. The acoustic waves radiate mainly in the downstream direction and plane waves are visibly attached to the shear layer. Acoustic waves of lower amplitude can be seen in the upstream direction. A zoom between $z = 0$ and $z = 15r_e$ is presented in figure 2 (b) for the density gradient norm and for the acoustic field. In the jet, the first shock is attached to the nozzle exit, and the shear layer is compressed. The first shock cell appears to be static whereas, downstream of $r = 9r_e$, shocks and compression waves seem to move. Finally, low-amplitude and high-frequency acoustic waves are observed near the nozzle exit, and higher-amplitude and lower-frequency acoustic waves are then attached to the shear layer.

IV. Aerodynamic results

A. Mean flow

The jet mean flow field is first described, and compared with data available in the literature. The fields of mean axial velocity $< u_z >$, mean radial velocity $< u_r >$ and mean static pressure $< p >$ are presented in figure 3. The sonic line corresponding to an axial Mach number $M_z =< u_z > /c$ equal to 1, where c is the local sound speed, is also plotted in figure 3(a). The sonic core length is thus $L_s = 36r_e$. In the similar jet considered using MARTEL experimental facility,[31] the end of the sonic core is around 50 radii which compares roughly with the present computation. As expected, shock cells are present in the mean radial velocity colormap in figure 3(b). Outside the flow field, the negative radial velocity is linked to the jet entrainment. Shock-cell structures are also observed in figure 3(c) resulting from the adaptation of the jet exit conditions to the ambient field conditions.

The variations of the inverse of the centerline velocity u_{axis} are plotted in figure 4(a). Data are made dimensionless according to the jet exit conditions. The end of the potential core L_c is located around $z = 20r_e$. In the experiment,[31] the end of the potential core is around 24 radii, which is consistent with the present computation. The numerical results from Nonomura & Fujii[5,6] are also in fair agreement with the current simulation. After the end of the potential core, the decrease of the jet centerline velocity exhibits a behaviour close to those observed in self-similar jets where velocity decay is given by $u_{axis}/u_j = 2Ar_j/(z - z_0)$, in which u_j and r_j are the fully expanded velocity and radius, A is the decay constant and z_0 denotes the virtual origin. In the present computation, A is equal to 4.90, which is lower than the usual value for unheated jets,[47] where A is between 5 and 6.5.

The variations of the centerline mean static pressure $< p >$ are plotted in figure 4(b), where six shock-cells are noticed. The shape of the three first shocks is consistent with measurements done by Norum & Seiner[48] on supersonic jets with an exit Mach number of $M_e = 2$ and equivalent perfectly-expanded Mach numbers of 1.67 and 1.80. The static pressure after the first shock on the jet centerline can be roughly estimated using straight shock formula. A pressure of 6.3×10^5 Pa is found from the jet exit conditions, which corresponds roughly to the simulation results in figure 4(b). In the present computation, the average shock-cell length L_{shock} is equal to $4.6r_e$. The shock-cell length can also be estimated by the formula of Tam and Tanna:[49]

$$L_{shock} = 2\pi(M_j^2 - 1)^{1/2} r_j/\mu_1 \tag{1}$$

where r_j is the fully expanded radius and $\mu_1 = 2.40483$. Using equation (1), it is found $L_{shock} = 5.6r_e$. The shock-cell length in the present computation is then smaller than that predicted by Tam and Tanna's model.[49] This might be due to the fact that the axial evolution of the shear layer thickness is not taken into account in equation (1).[21,50]

B. Turbulent flow

In this section, the turbulent fluctuations in the present jet are characterized to later enable possible acoustic sources. The root-mean-square (rms) variations of axial and radial velocities along the jet centerline and along the line $r = r_j$ are plotted in figure 5. Along the jet axis in figure 5(a), the velocity fluctuations

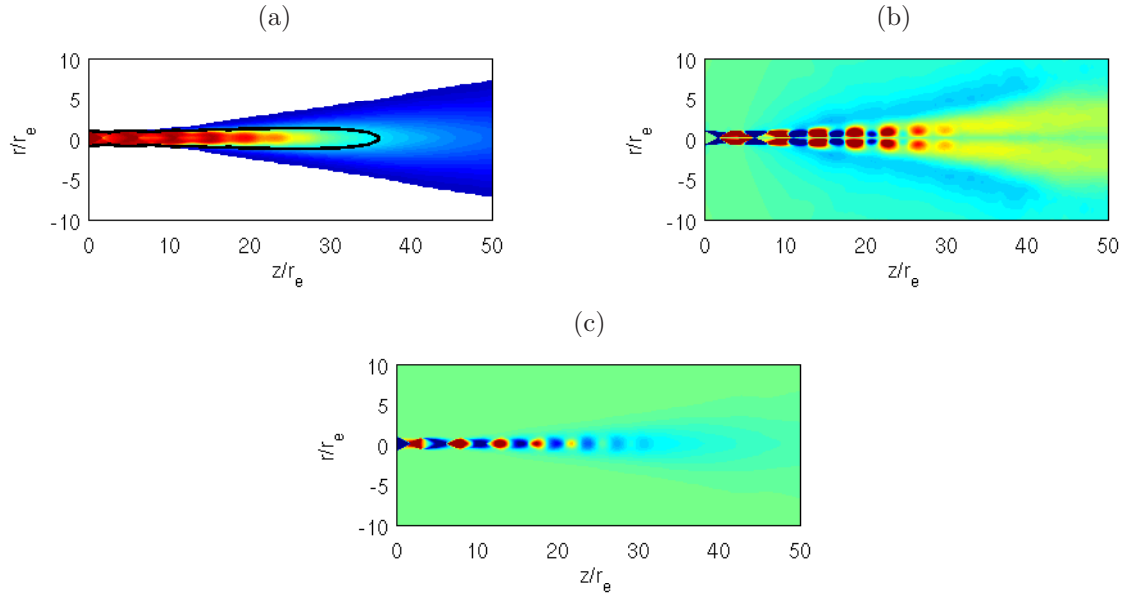

Figure 3. Representation in the (z, r) plane of (a) mean axial velocity $< u_z >$, (b) mean radial velocity $< u_r >$ and mean static pressure $< p >$. The color scale ranges for levels from 80 to 1255 m/s for $< u_z >$, from -30 to 30 m/s for $< u_r >$ and from 0.5×10^5 to 1.5×10^5 Pa for $< p >$. The sonic line is plotted in black on the mean axial velocity field.

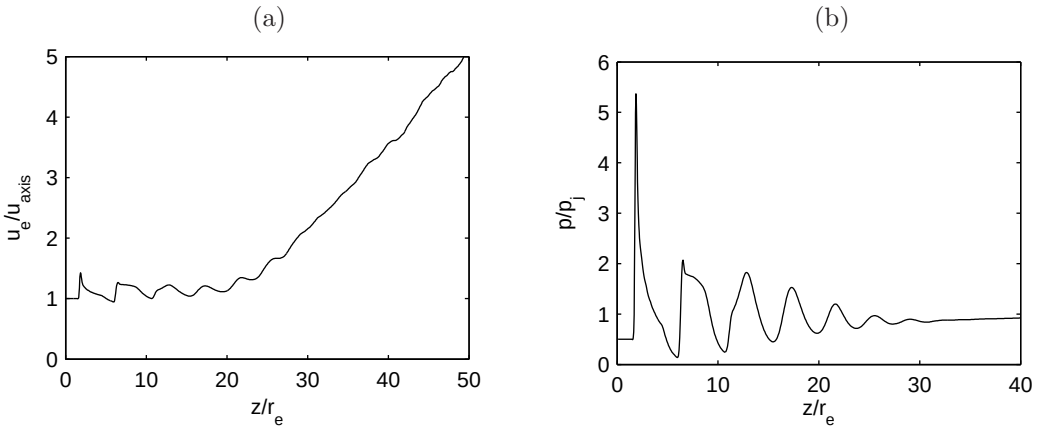

Figure 4. (a) Variations along the jet centerline of the inverse of the mean longitudinal velocity u_{axis}. (b) Variations of the mean static pressure $< p >$ along the jet centerline

first increase by step. The maximum of rms quantities for axial and radial velocities is reached around $z = 25r_e$ and a difference of amplitude is noticed between axial and radial velocity fluctuations. Along the shear layer in figure 5(b), low rms levels are observed between the nozzle exit and $z = 6r_e$. This trend might be explained by the low level of turbulence at the nozzle exit or by the shear layer distortion. In the same figure, axial velocity fluctuations exhibit a rapid growth around $z = 6.5r_e$. The peak location of rms quantities is before the end of the potential core for axial velocity fluctuations and after the end of the potential core for radial velocity fluctuations. Moreover, fluctuations of the axial velocity have a higher amplitude than fluctuations of radial velocity. This difference might be explained by compressible effects.[51] Finally, note that similarities are found for velocity fluctuations along the jet centerline and along the shear layer between the present computation and PIV measurements of Alkislar *et al.*[25] made on a rectangular screeching jet.

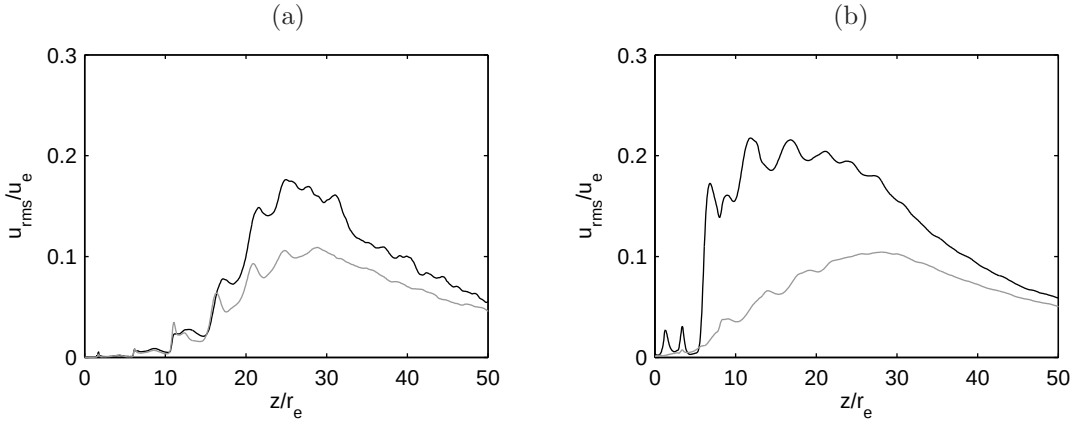

Figure 5. Variations of rms velocity fluctuations: ——— axial velocity fluctuations and ——— radial velocity fluctuations along (a) the jet centerline and (b) the line $r = r_j$.

To illustate the shear layer properties, the jet half-width $\delta_{0.5}$ and the local mean Mach number M_{shear} along the line $r = r_j$ are plotted in figure 6. The jet half-width $\delta_{0.5}$ is defined by $< u_z > (\delta_{0.5}) = u_{axis}/2$, and the mean local Mach number is $M_{shear} = \sqrt{< u_z >^2 + < u_r >^2}/c$. The jet half-width is modulated by the shock-cell structures in figure 6(a). Before the end of the potential core, the jet half-width is lower than r_e, thus the axial velocity fluctuations will be studied along the line $r = r_j$. Strong variations of the local mean Mach number are observed along the line $r = r_j$ in figure 6(b), and the amplitude of variations decreases in the axial direction. Such variations of the jet half-width and of the local mean Mach number are typically found in unperfectly expanded jets and should affect the turbulent structures.

The mean-square value of axial velocity fluctuations $< u_z'^2 >$ along the shear layer is now decomposed into its azimuthal components by applying two-dimensional Fourier transform to u_z'. This kind of decomposition has already been carried out for supersonic jets[29,30] in order to compare numerical results with linear stability prediction. The overall mean-square value and the contributions of the axisymmetric component $n = 0$ and of the components $n = 1$ and $n = 2$ are plotted in figure 7. In the early stage of the shear layer development, the contributions of azimuthal modes higher than 2 prevail. The modes $n = 1$ and $n = 2$ have nearly the same contribution before the end of the potential core, and they are more amplified than the axisymmetric component. The maximum contribution of the $n = 2$ component is reached near the end of the potential core, whereas the maximum contribution of the $n = 1$ component is reached downstream of the end of the potential core near $z = 24r_e$. Finally, the maximum contribution of the axisymmetric component is located near $z = 28r_e$. Tam *et al.*[7] and Seiner *et al.*[8] have shown by applying linear stability analysis to perfectly-expanded heated jets at an exit Mach number of $M_j = 2$ that the contributions of the $n = 1$ and $n = 2$ Kelvin-Helmholtz modes are close, and higher than the contribution of the axisymmetric Kelvin-Helmholtz mode.

Spectra of axial velocity fluctuations along the line $r = r_j$ are shown in figure 8 at $z = 6$, 12, 18, 24 and 30 radii as a function of the Strouhal number St_e defined by $St_e = 2fr_e/u_e$, where f is the frequency. Spectra are plotted in logarithmic scales, and for clarity, the levels are incremented of one order of magnitude as the axial position increases. At $z = 6r_e$, a peak located at $St_e = 0.3$ is noticed, whereas at other axial locations, the axial velocity spectra are more broadband.

The spectra obtained at $z = 6r_e$, $z = 12r_e$, $z = 18r_e$ and $z = 24r_e$ are now presented in linear scales

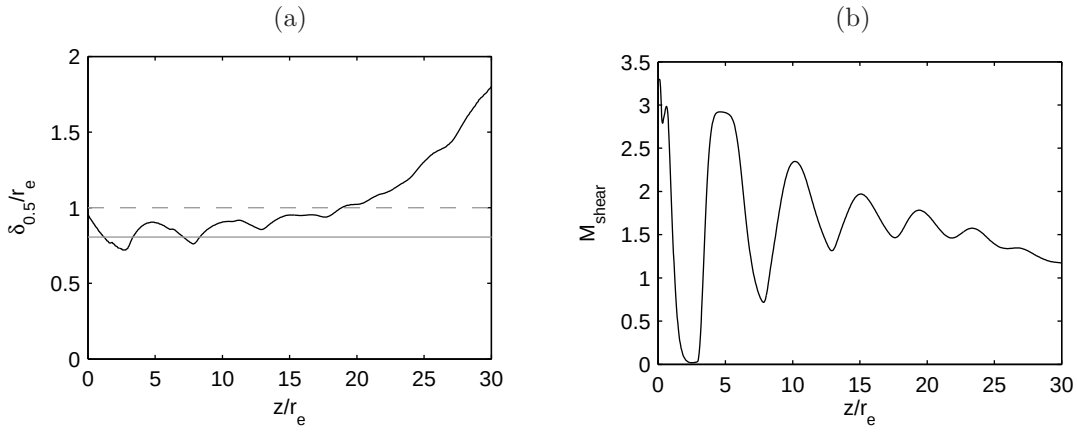

Figure 6. Axial evolution of (a) ——— the jet half-width $\delta_{0.5}$ and of (b) ——— the local mean Mach number M_{shear} along the line $r = r_j$. ——— line $r = r_j$ and – – – line $r = r_e$.

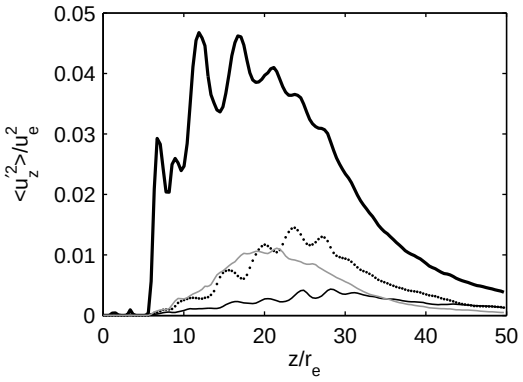

Figure 7. Axial evolution of the mean square value of the fluctuating axial velocity $< u_z'^2 > /u_e^2$ and the contribution of azimuthal components $n = 0$, $n = 1$ and $n = 2$ along the line $r = r_j$. ——— overall value, ——— contribution of the axisymmetric component $n = 0$, ····· contribution of the $n = 1$ component and ——— contribution of the $n = 2$ component.

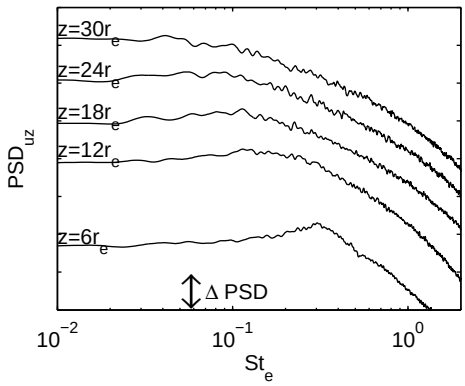

Figure 8. Power spectral density in logarithmic scales of axial velocity fluctuations along the line $r = r_j$ at $z = 6r_e$, $z = 12r_e$, $z = 18r_e$, $z = 24r_e$ and $z = 30r_e$. For the sake of clarity, the levels are incremented of ΔPSD with the distance. ΔPSD denotes one order of magnitude.

in figure 9, together with the contributions of $n = 0$, 1 and 2 azimuthal components. At $z = 6r_e$, the contributions of modes $n = 0$, 1 and 2 are negligible, thus the maximum at $St_e = 0.3$ is associated with azimuthal modes of orders higher than 2. At $z = 12r_e$, the maximum is close to $St_e = 0.11$ and, the $n = 1$ and $n = 2$ components have emerged. Before the end of the potential core, at $z = 18r_e$, the maximum of axial velocity fluctuations is still located at $St_e = 0.11$, and an harmonic is noticed at $St_e = 0.22$. Moreover a peak around $St_e = 0.08$ is well marked. For the peaks at $St_e = 0.08$ and $St_e = 0.11$, the contributions of the $n = 1$ and $n = 2$ components are similar, but for the harmonic frequency at $St_e = 0.22$, the contribution of the $n = 2$ component is more important. Downstream of the end of the potential core, at $z = 24r_e$, low-frequency peaks at $St_e = 0.05$, $St_e = 0.08$ and $St_e = 0.09$ dominate the spectrum of axial velocity fluctuations, but the peak at $St_e = 0.11$ is still present. At this axial location, the contribution of the first azimuthal mode is the most important, and its maximum is reached at $St_e = 0.08$. Finally, it can be noticed that the contribution of the axisymmetricmode is higher with respect to the previous axial positions, and its maximum is near $St_e = 0.04$. Different peaks are thus observed for axial velocity fluctuations along the line $r = r_j$. This trend might be due to the quasi-laminar shear layer at the nozzle exit resulting in a moderate Reynolds number jet behaviour.[52] Moreover, the presence of shock cells in the jet plume should also force the turbulence.

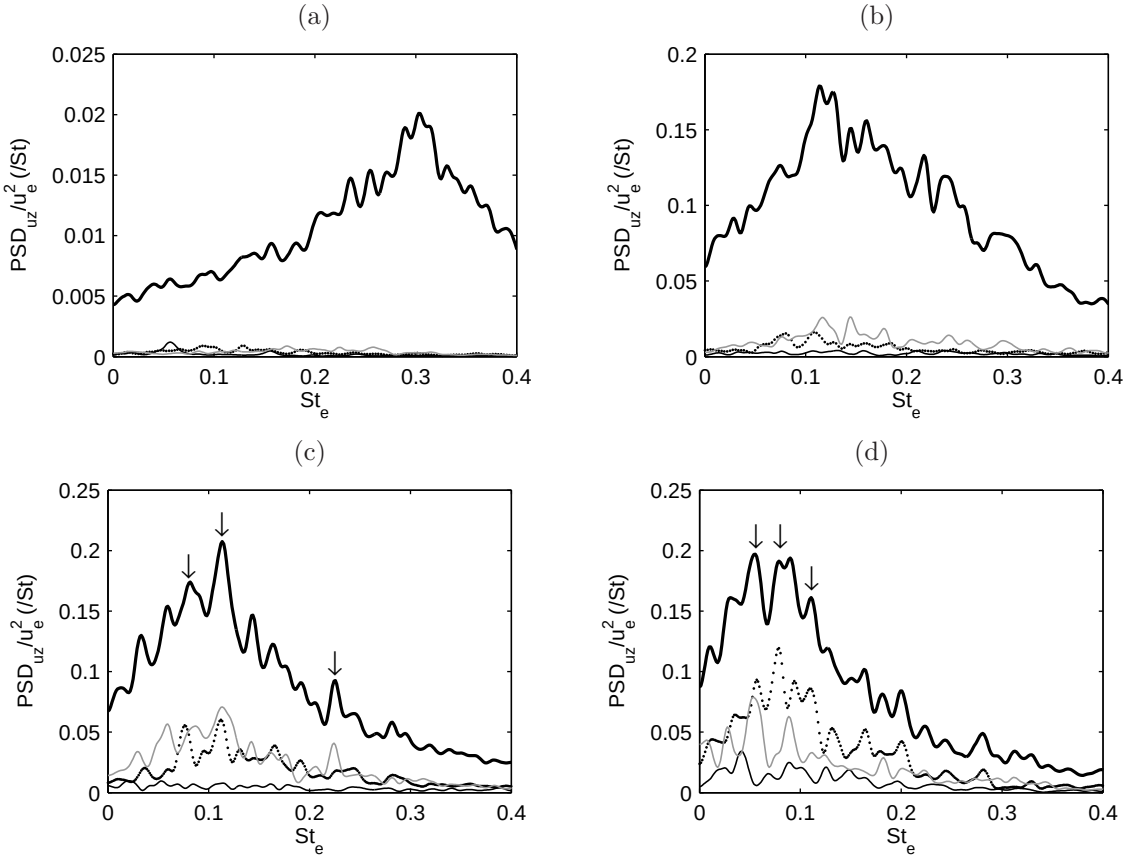

Figure 9. Power spectral density (PSD) of axial velocity fluctuations along the line $r = r_j$ at (a) $z = 6r_e$, (b) $z = 12r_e$, (c) $z = 18r_e$ and (d) $z = 24r_e$. ——— Overall value, ——— contribution of the axisymmetric component $n = 0$, ····· contribution of the component $n = 1$ and ——— contribution of the component $n = 2$.

To investigate the perseverence of peak Strouhal numbers observed in figure 9, the Strouhal numbers of the maximum of the axial velocity spectra along the line $r = r_j$ are reported in figure 10(a) as a function of the axial position. A decrease by step of the peak Strouhal number is noticed, which is different from the continuous decay of the peak Strouhal number observed in perfectly-expanded supersonic jets by Papamoschou *et al.*[53] Strouhal numbers of 0.3, 0.11 and 0.05 are therefore persistent. Axial velocity fluctuations at a Strouhal number of 0.3 are dominant between $z = 6r_e$ and $z = 9r_e$, then the peak Strouhal number decreases down to 0.11. A large step at $St_e = 0.11$ is observed between $z = 12.5r_e$ and $20.5r_e$, and near the end of the potential core, the peak Strouhal number switches to a value close to 0.05. Note that

the decrease of the peak Strouhal number downstream of $z = 9r_e$ also corresponds to a change of shock-cell dynamics in figure 2(b). For the peak switching near the end of the potential core, a similar behaviour has already be pointed out in a plane supersonic screeching jet.[21] Therefore, in the present computation, the presence of shock cells likely affects the turbulence structures. For the axial velocity fluctuations along the line $r = r_j$, the peak Strouhal numbers of the contributions of modes $n = 1$ and $n = 2$ are reported in figure 10(b). From $z = 11r_e$ to $z = 20r_e$, peak Strouhal numbers are mostly found between $St_e = 0.1$ and $St_e = 0.17$, then the peak Strouhal number switches to $St_e = 0.08$ for the mode $n = 1$ and to $St_e = 0.05$ for the mode $n = 2$ after the potential core. Moreover, peaks around $St_e = 0.08$ for the $n = 1$ azimuthal component are also observed sometimes before the end of the potential core.

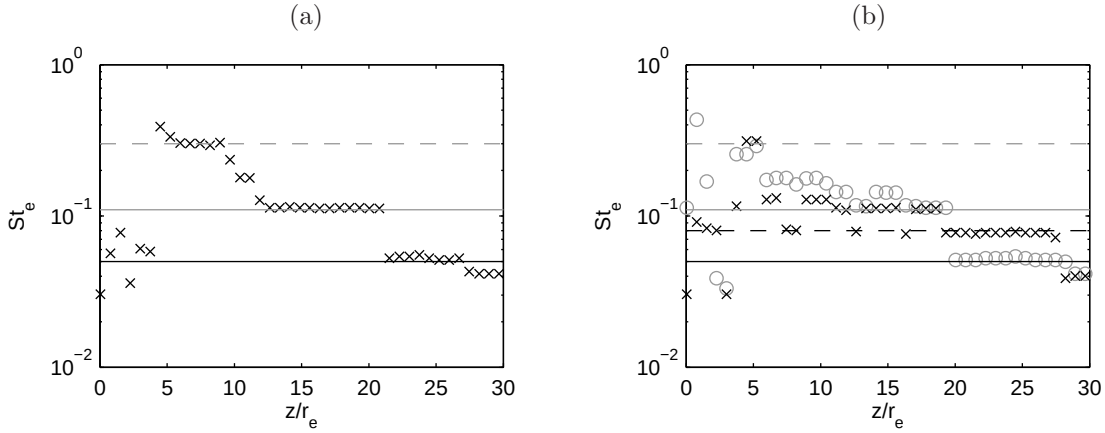

Figure 10. Peak Strouhal number of axial velocity fluctuations along the line $r = r_j$. (a) × peak Strouhal number of the power spectral density and (b) peak Strouhal number of × $n = 1$, and ○ $n = 2$ azimuthal components. ——— $St_e = 0.05$, − − − $St_e = 0.08$, ——— $St_e = 0.11$ and − − − $St_e = 0.3$.

V. Acoustic results

A. Acoustic near field

The properties of the acoustic near field is first compared to experimental data, and then investigated using two-dimensional Fourier transform in order to display links with turbulence within the shear layer. The overall sound pressure level (OASPL) is plotted in figure 11 with experimental data from Greska *et al.*[54] at a distance of 9.5 radii from the jet axis, and from Varnier & Gély[31] and Greska *et al.*[54] at a distance of 16 radii from the jet centerline. The experimental jet of Greska *et al.*[54] is fully expanded, with an exit Mach number M_j of 2, and an acoustic Mach number of $M_a = 3$. The exit conditions of the experimental jet of Varnier & Gély[31] are presented in table 1. The OASPL of the present simulation is in fair agreement with experimental data. The jet radiates mainly in the downstream direction. At $r = 9.5r_e$ from the jet axis, the maximum is located at $z = 30r_e$, and a rapid growth of OASPL is observed between $z = 7r_e$ and $z = 20r_e$. At $r = 16r_e$ from the jet centerline, a difference of 5 dB is observed between the present computation and measurements of Varnier & Gély[31] in the downstream direction. It be explained by differences in Reynolds number[55] and in nozzle exit conditions.[56,57]

The acoustic near-field is now investigated at 9.5 radii from the jet centerline. An azimuthal decomposition of the acoustic near field is first carried out. The cross-correlation function R^θ of the fluctuating pressure p' at point (r, θ, z) is defined by:

$$R^\theta(\delta\theta) = \frac{< p'(\theta)p'(\theta + \delta\theta >}{< p'^2(\theta) >^{1/2} < p'^2(\theta + \delta\theta) >^{1/2}} \tag{2}$$

where $\delta\theta$ is the azimuthal separation. The cross-correlation function R^θ obtained along the line $r = 9.5r_e$ is then decomposed into a Fourier sum[57] as follows:

$$R^\theta(\delta\theta) = \sum_{n=0}^{\infty} a_n^\theta \cos(n\delta\theta) \tag{3}$$

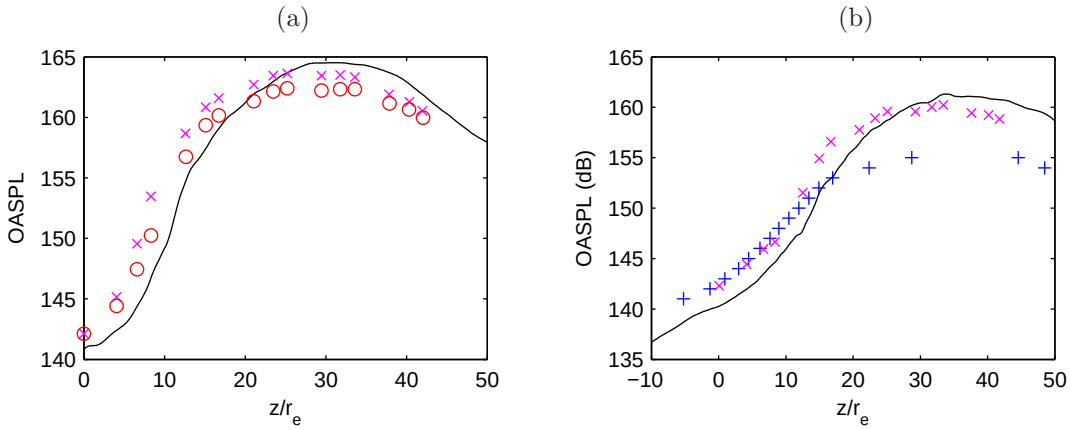

Figure 11. Variations of the overall sound pressure level (OASPL). (a) ——— Present computation at $r = 9.5r_e$, measurements of Greska *et al.*:[54] × at $r = 8r_e$ and o at $r = 10r_e$ and (b) ——— present computation at $r = 16r_e$, × measurements of Greska *et al.*[54] at $r = 16r_e$ and + measurements of Varnier & Gély[31] at $r = 16r_e$.

where a_n^θ is the relative amplitude of the Fourier mode n. The coefficients of the axisymmetric component, $n = 0$, and of the $n = 1$ and 2 components are presented in figure 12. Up to $z = 30r_e$, the mode $n = 1$ dominates the modes $n = 0$ and $n = 2$, and downstream of $z = 30r_e$, the axisymmetric mode $n = 0$ has the highest amplitude. The similar trend has also been observed by Bodony *et al.*[58] in a jet at an exit Mach number of $M_e = 1.95$ and an equivalent fully-expanded Mach number of $M_j = 2.2$. Moreover, it could be noticed that between $z = 8$ and $z = 18$ radii, the acoustic field is less correlated. According to figure 11(a), this region corresponds to the rapid growth of OASPL. In the jet shear layer, the contributions of $n = 1$ and $n = 2$ components have been found to be more important than the contribution of the axisymmetric mode for axial velocity fluctuations in figure 7, thus the $n = 2$ azimuthal component may not be an efficient noise source.

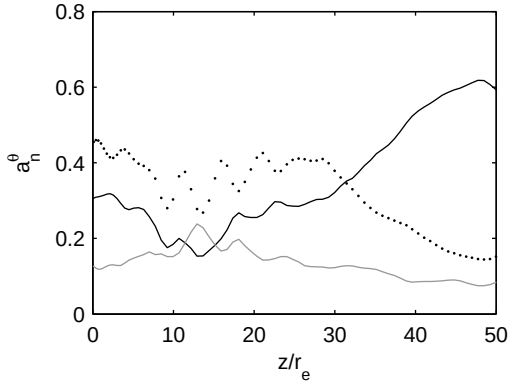

Figure 12. Variations in the axial direction of the coefficients a_n^θ obtained from the azimuthal decomposition of cross-correlation R^θ of fluctuating pressure at $r = 9.5r_e$: ——— axisymmetric component $n = 0$, ····· component $n = 1$, and ——— component $n = 2$.

Near-field acoustic spectra are presented in figure 13 at axial locations $z = 0$, $z = 10r_e$, $z = 15r_e$ and $z = 20r_e$. In the upstream direction, at $z = 0$, a double peak at $St_e = 0.08$ and $St_e = 0.095$ dominates the acoustic spectrum, and a peak of lower amplitude is observed around $St_e = 0.05$. Peaks at $St_e = 0.05$ and $St_e = 0.08$ are still found at the different axial locations. A broadband high-frequency noise centered around $St_e = 0.3$ has emerged at $z = 10$ radii. This broadband component seems to be persistent at $z = 15$ radii. Moreover, from $z = 0$ to 15 radii, a peak moving from $St_e \approx 0.1$ to $St_e \approx 0.13$ is noticed. At $z = 20$, the peak at $St_e = 0.08$ is still present, but a broadband component between $St_e = 0.1$ and $St_e = 0.2$ prevails. Axial velocity fluctuations at $St_e = 0.3$, 0.08 and 0.05 have also been observed along the shear layer in figure 10. Velocity fluctuations at $St_e = 0.3$ are located in the first shock cell and associated with azimuthal modes higher than 2, whereas velocity fluctuations at $St_e = 0.08$ are connected to the $n = 1$ azimuthal

component. Finally, velocity fluctuations at $St_e = 0.05$ have been noticed after the end of the potential core in figure 10(a).

To characterize noise sources, the formula proposed by Tam *at al.*[22] to predict the peak frequency of the upstream propagating shock-associated noise is reported in figure 13. The estimation of the peak frequency is given by:

$$f_{up} = \frac{u_c}{L_{shock}(1 + M_c)} \tag{4}$$

the convection velocity u_c and the mean shock-cell length L_{shock} are estimated from the LES fields. The convection velocity is calculated from the correlation function between signals of axial velocity fluctuations u'_z at two points separated by the distance $2r_e$. Along the line $r = r_j$, the mean value between $z = 6r_e$ and the end of the potential core is equal to $u_c = 0.53$ which is coherent with usual values in axisymmetric jets.[18] It is thus found $St_{up} = 2r_e f_{up}/u_e = 0.08$ which is in fair agreement with the peak observed at the same location in figure 10(b) and figure 13. Fluctuations at this Strouhal number in the jet plume may be linked with shock-turbulence interactions, and the resulting peak in the acoustic field at $z = 0$ is thus identified as upstream propagating shock-associated noise. In a plane screeching jet, Berland *et al.*[21] have observed a peak at a lower Strouhal number than the screech fundamental in acoustic spectra in the upstream direction. Morever, they found that this low-frequency acoustic peak has the same Strouhal number than velocity fluctuations after the end of the potential core. This low-frequency peak has also been noticed in experimental spectra,[23,59] and Tam[18] has attributed it to a trace of the turbulent mixing noise occuring near the end of the potential core. The present near-field spectra can be qualitatively compared to near-field measurements done by Seiner & Yu[19] for an overexpanded jet at an exit Mach number of 1.45. The moving peak from $St_e \approx 0.1$ to $St_e \approx 0.13$ may thus be idendified as broadband shock-associated noise. Finally, the broadband noise centered at $St_e = 0.3$ in figure 13 may be radiated by shear-layer fluctuations at the same Strouhal number near the nozzle exit. This assumption is enhanced by the pressure snapshot in figure 2.

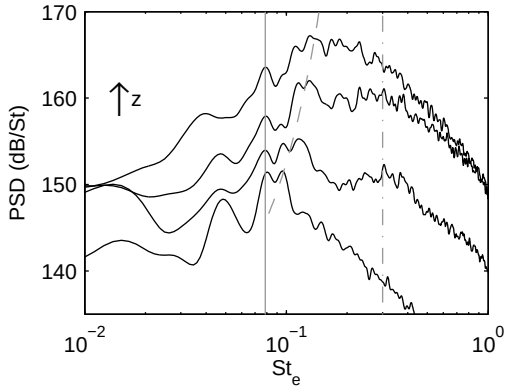

Figure 13. Near-field acoustic spectra at $r = 9.5r_e$. From bottom to top: $z = 0$, $z = 10r_e$, $z = 15r_e$ and $z = 20r_e$. ——— Estimation of the upstream propagating shock associated noise using equation 4, — · — · $St_e = 0.3$ and — — — moving peak.

An azimuthal decomposition of acoustic spectra at $z = 0$ and $z = 10r_e$ is presented in figure 14. At $z = 0$, peaks at $St_e = 0.05$ and $St_e = 0.08$ are respectively associated with the axisymmetric and the $n = 1$ azimuthal components. A peak at $St_e = 0.15$ dominated by the $n = 2$ component is also observed. This peak may be an harmonic of the peak at $St_e = 0.08$. In the jet, peaks of velocity fluctuations at $St_e = 0.08$ connected to the mode $n = 1$ has previously been remarked in figure 10(b). Berland *et al.*[21] have observed similar spatial distributions between the screech tone and velocity fluctuations along the shear layer at the screech fundamental frequency. This supports the indentification of the noise component at $St_e = 0.08$ as shock/turbulence interactions. For the present computation, the backloop mechanism which characterizes the screech noise has not been identified yet. The azimuthal properties of the peak at $St_e = 0.05$ enhances the hypothesis that this component is linked with turbulent mixing noise because the acoustic waves radiated by turbulent mixing near the end of the potential core has the particularity to be mostly axisymmetric.[60]

At $z = 10r_e$, peaks at $St_e = 0.05$ and $St_e = 0.08$ are still respectively connected to the axisymmetric and $n = 1$ azimuthal components. The broadband noise centered at $St_e = 0.3$ in figure 13 is azimuthally less correlated. Based on this observation, Mach waves can be responsible for this noise component because

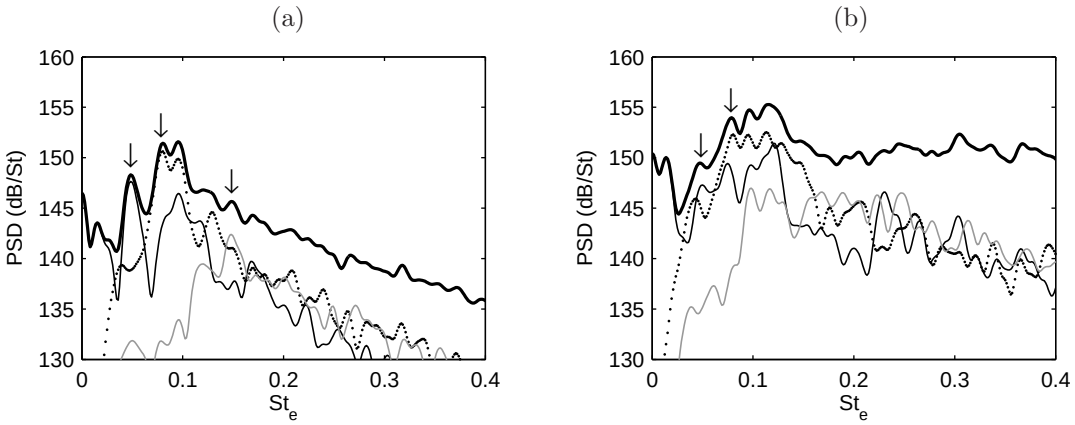

Figure 14. Azimuthal decomposition of the near-field acoustic spectra at (a) $(r, z) = (9.5r_e, 0)$ and (b) $(r, z) = (9.5r_e, 10r_e)$. ——— power spectral density, ——— contribution of the axisymmetric component $n = 0$, ····· contribution of the component $n = 1$ and ——— contribution of the component $n = 2$.

less coherent velocity fluctuations at $St_e = 0.3$ have also been observed in the shear layer between $z = 6$ and $z = 9$ radii in figure 7 and in figure 10.

Near-field acoustic spectra in the downstream direction are now investigated in figure 15 at $z = 30$ and $z = 40$ radii. The overall acoustic spectrum and the contribution of modes $n = 0$, 1 and 2 are first shown in figure 15(a) at $z = 30r_e$. This axial location corresponds to the maximum of the OASPL plotted in figure 11(a). The acoustic spectrum is broadband, and its maximum is located around $St_e = 0.13$. The $n = 1$ azimuthal component is dominant at the maximum location, however the contribution of the axisymmetric mode cannot be neglected. In addition, the Strouhal of the spectrum maximum corresponds roughly to peaks Strouhal number observed for $n = 1$ component in figure 10(b) between $z = 9r_e$ and $z = 20r_e$. Therefore the mode $n = 1$ might be radiated by Mach wave mechansim. At $z = 40r_e$, axisymmetric and low-frequency acoustic waves clear prevail, and two peaks are noticed. The first one is located around $St_e = 0.05-0.06$, and the second one is located at $St_e = 0.1$. Peaks at $St_e \approx 0.05$ have also been observed in velocity fluctuations spectra after the end of potential core in figure 10 (a). This noise component may thus be identified as turbulent mixing noise. The Strouhal number of the second peak in figure 15(b) is in fair agreement with peak Strouhal numbers observed between $z = 12.5$ and $z = 20.5$ in figure 10(a). However, the contribution of the axisymmetric mode to axial velocity fluctuations along the line $r = r_j$ has been found to be very low in figure 7. Further work would be necessary to understand the radiation mechanism of this axisymmetric noise component.

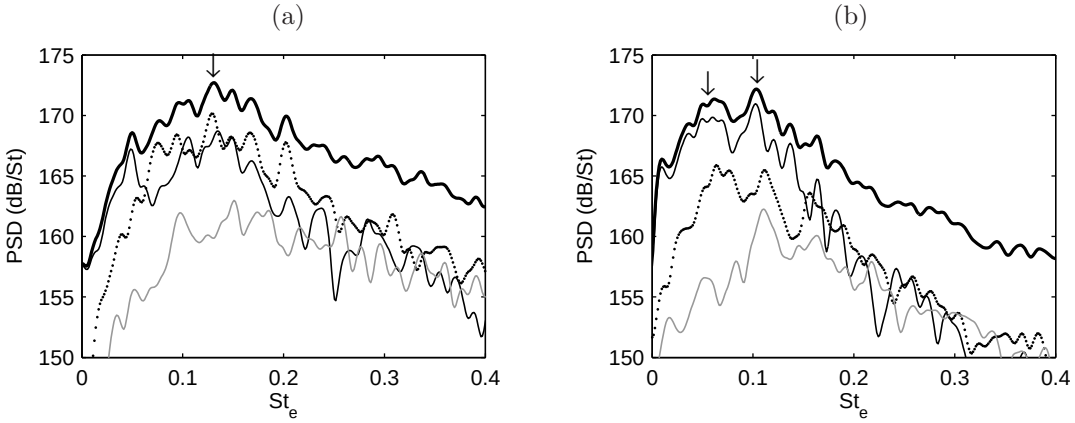

Figure 15. Azimuthal decomposition of the near-field acoustic spectra at (a) $(r, z) = (9.5r_e, 30r_e)$ and (b) $(r, z) = (9.5r_e, 40r_e)$. ——— power spectral density, ——— contribution of the axisymmetric component $n = 0$, ····· contribution of the $n = 1$ component and ——— contribution of the $n = 2$ component.

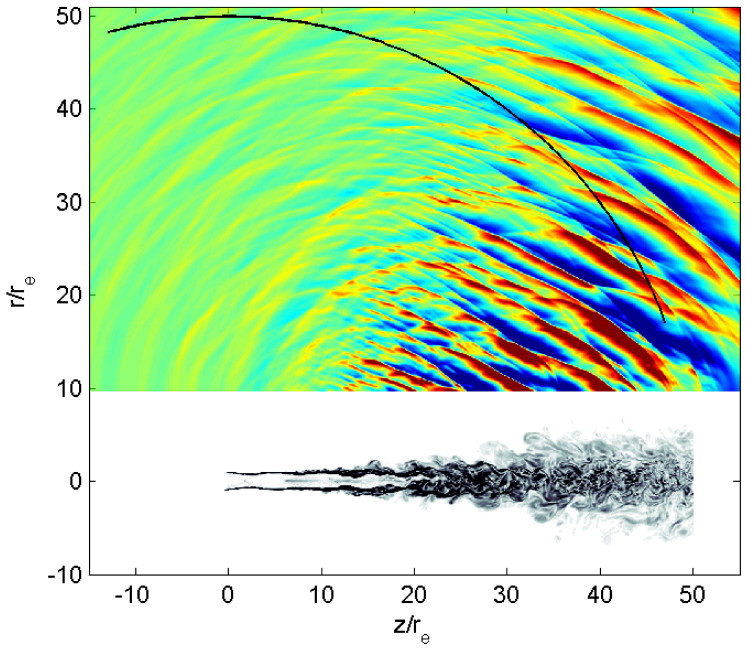

Figure 16. Snapshots in the (z, r) plane of vorticity in the jet and of fluctuating pressure propagated using Euler equations. The color scale ranges for levels from -3000 to 3000 Pa for the fluctuating pressure. ——— Position where pressure signals are recorded.

B. Acoustic far field

The LES data obtained on a control surface located at $r = 9.5r_e$ are propagated to 50 radii from the nozzle exit solving Euler equations using low-dissipation schemes[34] in combination with an adaptative shock-capturing method.[35] Full Euler equations are used to take into account the non-linear propagation of sound waves. A snapshot of acoustic pressure is shown in figure 16. Acoustic waves propagate mainly in the downstream direction, but upstream-propagating waves are also noticed. A line at 50 radii from the nozzle exit where pressure signals are recorded is plotted in black.

The OASPL is presented at this distance in figure 17 according to the directivity angle θ. The reference of the angle θ is taken into the flow direction. As it has already been established in figure 11 , the axisymmetric and the $n = 1$ azimuthal components dominate the acoustic field. From $\theta = 20°$ to $40°$, the axisymmetric mode prevails, then from $\theta = 40°$ to $60°$, the $n = 0$ and $n = 1$ azimuthal components have nearly the same contribution to the acoustic field. Between $\theta = 60°$ and $70°$, the acoustic field is azimuthally less correlated, and finally, for θ angles larger than $70°$, the contributions of the mode $n = 1$ dominate the acoustic field.

Acoustic spectra at $\theta = 20°$, $40°$, $65°$ and $90°$ are shown in figure 18. In the downstream direction, at $\theta = 20°$, the acoustic field is mostly axisymmetric, and the acoustic spectrum is dominated by low-frequency waves between $St_e \approx 0.05$ and $St_e = 0.1$. The maximum of the mode $n = 1$ is located around $St_e = 0.08$. For an angle θ of $40°$, the maximum of the spectrum is observed at $St_e = 0.12$, and peaks at $St_e = 0.08$ both for the axisymmetric and the $n = 1$ components are noticed. At $\theta = 65°$, The acoustic spectrum is broadband and azimuthally less correlated. Finally, at $\theta = 90°$, the maximum of the spectrum is located around $St_e = 0.15$, and is dominated by the mode $n = 1$.

The peak Strouhal numbers of the acoustic spectra at different θ locations are reported in figure 19. In the downstream direction, the peak Strouhal numbers range from $St_e = 0.1$ to $St_e = 0.15$, and the peak at $St_e = 0.1$ is persistent from $\theta = 21°$ up to $\theta = 35°$. After $\theta = 65°$, the peak Strouhal number decreases from $St_e = 0.25$ down to $St_e = 0.13$. The formula of Tam & Tanna[49] is used to estimate the central frenquency of the broadband shock noise as a function of the directivity:

$$f_{shock} = \frac{u_c}{L_{shock}(1 - M_c \cos(\theta))} \tag{5}$$

A rough agreement is observed in figure 19 between formula (5) and the peak Strouhal number obtained in the present computation. However recorded data are not really in far field. Therefore, the formula is now

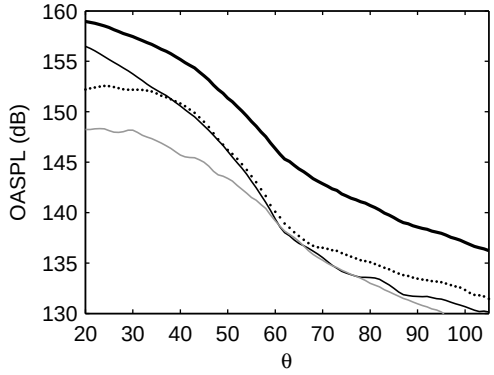

Figure 17. Far-field overall pressure level and its azimuthal decomposition according to the directivity θ. ——— OASPL, ——— axisymmetric $n = 0$ component, ····· $n = 1$ component and ——— $n = 2$ component.

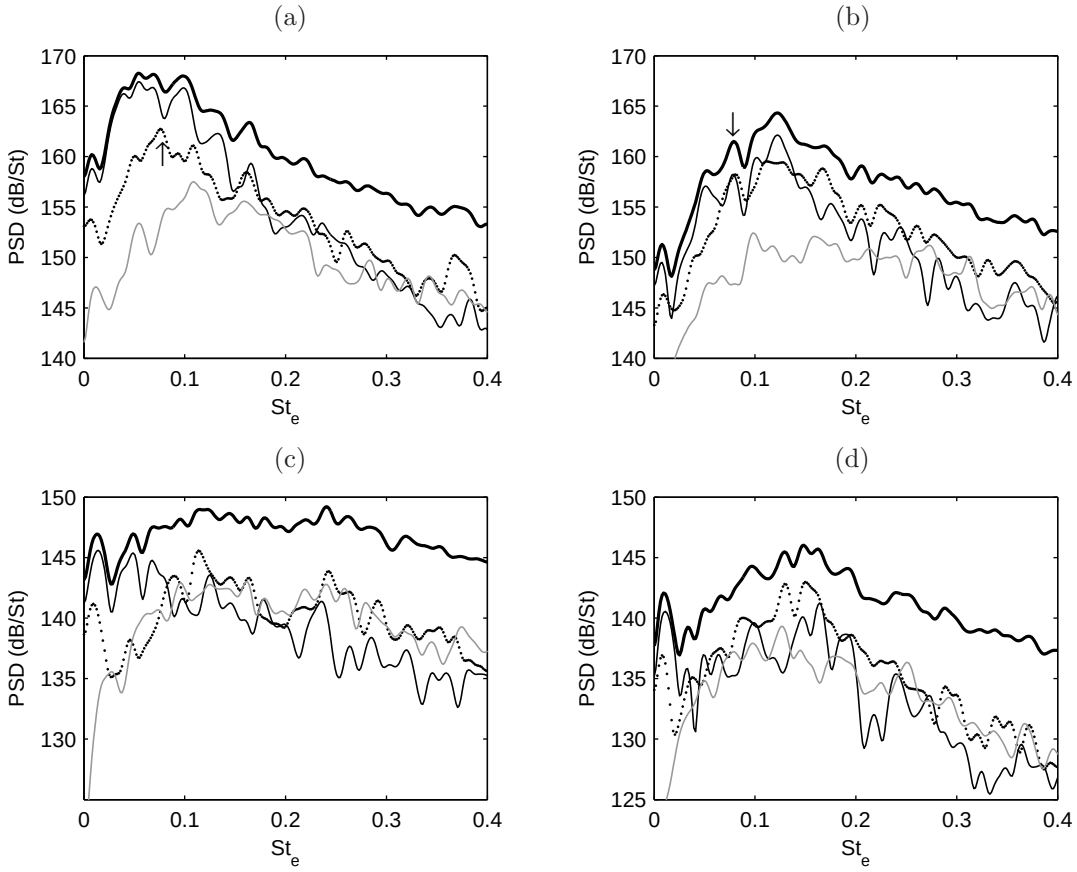

Figure 18. Far-field acoustic spectra at $\theta = 20°$, $\theta = 40°$, $\theta = 65°$ and $\theta = 90°$. ——— power spectral density, ——— contribution of the axisymmetric component $n = 0$, ····· contribution of the component $n = 1$ and ——— contribution of the component $n = 2$.

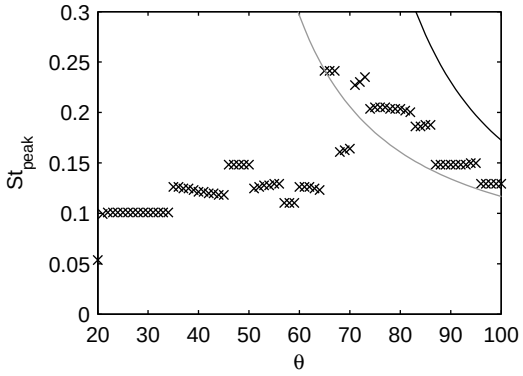

Figure 19. Peak Strouhal number of the acoustic far-field power spectra density as a function of the directivity θ. $\times$ peak Strouhal number and prediction of the central frequency of shock associated noise given by equation 5: ——— without origin correction and ——— with origin correction.

plotted by taking the end of the potential core as the origin. A better agreement is found with computational data that may indicate the predominance of shock-associated noise in the sideline and upstream directions.

VI. Conclusion

In the present paper, a compressible three-dimensional large-eddy simulation is performed for a circular overexpanded propulsive jet using low-dissipation and low-dispersion schemes and an adaptative shock-capturing procedure. Numerical results are presented, and qualitatively compared with literature data. A fair agreement is observed for the near-field overall pressure levels between the present computation and experimental data.[31,54]

The shear-layer velocity fluctuations exhibit similar properties than turbulence in screeching jets, and show persistent axial velocity components at Strouhal numbers of 0.3 and 0.11 upstream the end of the potential core and of 0.05 downstream the end of the potential core. Velocity fluctuations at $St_e = 0.3$ are observed in the first shock cell, and they are connected to azimuthal modes higher than 2. the decrease of peak velocity frequency from $St_e = 0.3$ down to $St_e = 0.11$ also corresponds to a change of shock motion. Axial velocity fluctuations near the end of the potential core are found azimuthally correlated, and the contributions of the first and the second azimuthal modes are more important thant the contribution of the axisymmetric mode. Finally, maxima of the first azimuthal mode often fluctuate at a Strouhal number around 0.08 in the jet shear layer.

The jet acoustic field is mainly described from near-field data. The acoustic field is dominated by the axisymmetric and first azimuthal modes, and different noise mechanisms such as shock-associated noise, Mach waves and turbulent mixing noise occuring near the end of potential core are identified. The upstream propagating shock-associated noise is connected to the first azimuthal mode, and its peak propagates around $St_e = 0.08$. For the moment, no feedback loop has been evidenced. A Mach wave component is generated by velocity fluctuations with azimuthal modes higher than 2 at the first shock cell. Mach waves radiated by the first azimuthal mode seem also to be present in the downstream direction. However, the distinction between Mach waves and shock-associated noise is not clear for this azimuthal component. Finally, an axisymmetric noise component at the same Strouhal number than the peak of velocity fluctuations after the end of the potential core is observed. This component is considered as turbulent mixing noise. A final noise component is radiating in the downstream direction at a Strouhal number of 0.1, and is associated with the axisymmetric mode. Its origin will be investigated in future works.

Acknowledgments

The first author is grateful to the Centre National d'Etudes Spatiales (CNES) for financial support. This work was granted access to the HPC resources of IDRIS under the allocation 2010-020204 made by GENCI (Grand Equipement National de Calcul Intensif).

References

[1]Oertel, H., "Mach wave radiation of hot supersonic jets investigated by means of the shock tube and new optical techniques," *Proc. 12th Inter. Symp. on shock tubes and waves*, Jerusalem, 1980, pp. 266-275.

[2]Varnier, J., "Experimental study and simulation of rocket engin free jet noise," *AIAA Journal*, Vol. 39, No. 10, 2001.

[3]Seiner, J., Ponton, M., Jansen, B. and lagen, N. "The effects of temperature on supersonic jet noise emission," AIAA/DLR Paper 92-02-046, 1992.

[4]Krothapalli, A., Greska, B. and Wishart D., "Aeroacoustics of a heated Mach 2.0 Jet," AIAA Paper 2005-2931, 2005.

[5]Nonomura, T. and Fujii K., "Over-expansion effects on Mach 3.0 supersonic jet acoustics," AIAA Paper 2008-2836, 2008.

[6]Nonomura, T. and Fujii K., "Mach number and temperature effects on Mach wave emission from supersonic jets," AIAA Paper 2008-6587, 2008.

[7]Tam, C.K.W, Chen, P. and Seiner, J.M., "Relation ship between instability waves and noise of high-speed jets," *AIAA J.*, Vol. 30, 1992, pp. 1747-1752.

[8]Seiner, J., Bhat, T. and Ponton, M., "Mach wave emission from high-temperature supersonic jet," *AIAA Journal*, Vol. 32, No. 12, 1994, pp. 2345-2350.

[9]McLaughlin, D.K., Morrison, G.L. and Troutt, T.R., "Experiments on instability waves in a supersonic jet and their acoustic radiation," *Journal of Fluid Mechanics*, Vol. 69, 1975, pp. 73-95.

[10]Krothapalli, A., Arakeri, V. and Greska, B., "Mach wave radiation: a review and an extension," AIAA Paper 2003-1200, 2003.

[11]Tam, C.K.W., Viswanathan, K., Ahuja, K.K. and Panda, J., "The sources of jet noise: experimental evidence," *Journal of Fluid Mechanics*, Vol. 615, 2008, pp. 253-292.

[12]Tam, C.K.W., Golbiowski, M. and Seiner, J.M., "On the two components of turbulent mixing noise from supersonic jets," *AIAA Paper*, 96-1716, 1996.

[13]Viswanathan, K., "Analysis of the two similarity components of turbulent mixing noise," *AIAA J.*, Vol. 40, 2002, pp. 1735-1744.

[14]Bogey, C. and Bailly, C. , "Investigation of downstream and sideline subsonic jet noise using large eddy simulation," *Theor. and Comp. Fluid Dynam.*, Vol. 20, 2006, pp. 23-40.

[15]Panda, J. and Seasholtz, R.G., "Experimental investigation of density fluctuations in high-speed jets and correlation with generated noise," *Journal of Fluid Mechanics*, Vol. 450, 2002, pp. 97-130.

[16]Bogey, C. and Bailly, C., "An analysis of the correlations between the turbulent flow and the sound pressure field of subsonic jets," *Journal of Fluid Mechanics*, Vol. 583, 2007, pp. 71-97.

[17]Tam, C.K.W. and Burton, D.E., "Sound radiated by instability waves of a supersonic flows. Part 2. Axisymmetric jets," *Journal of Fluid Mechanics*, Vol. 138, 1984, pp. 273-295.

[18]Tam, C., "Supersonic jet noise," *Annu. Rev. Fluid Mech.*, Vol. 27, 1995, pp. 17-43.

[19]Seiner, J.M. and Yu, J.C., "Acoustic near-field properties associated with broadband shocknoise," *AIAA Journal*, Vol. 22, No. 9, 1984, pp. 1207-1215.

[20]Tanna, H.K., "An experimental study of jet noise. Part II: shock associated noise", *Journal of Sound and Vibrations*, Vol. 30, No. 3, 1977, pp. 429-444.

[21]Berland, J., Bogey, C. and Bailly, C., "Numerical Study of screech generation in a planar supersonic jet," *Physics of Fluids*, Vol. 19, No. 7, 2007.

[22]Tam, C., Seiner, J. and Yu, J., "Proposed relationship between broadband shock associated noise and screech tones," *Journal of Sound and Vibration*, Vol. 110, No. 2, 1986, pp. 309-321.

[23]Raman, G., "Compressible effects in a turbulent annular mixing layer. Part 1. Turbulence and growth rate," *Journal of Fluid Mechanics*, Vol. 336, 1997, pp. 69-90.

[24]Powell, A., "On the mechanism of chocked jet noise," *Proc. Phys. Soc. London*, Sect. B 66, 1039, 1953.

[25]Alkislar, M.B., Krothapalli, A. and Lourenco, L.M., "Strucutre of screeching rectangular jet: a stereoscopic particule image velocimetry study," *Journal of Fluid Mechanics*, Vol. 489, 2003, pp. 121-154.

[26]Panda, J., "An experimental investigation of screech noise generation," *Journal of Fluid Mechanics*, Vol. 378, 1999, pp. 71-96.

[27]Mankbadi, R.R., Hixon, R., Shih, S.H. and Povinelli, L.A., "Use of linearized Euler equations for supersonic jet noise prediction", *AIAA J.*, Vol. 36, No. 2, 1998, pp. 140-147.

[28]Freund J.B, Lele, S.K. and Moin, P., "Numerical simulation of a Mach 1.92 turbulent jet and its sound field," *AIAA Journal*, Vol. 38, No. 11, 2000, pp. 2023-2031.

[29]Mohseni, K., Colonius, T. and Freund, J.B., "An evaluation of linear instability waves as sources in a supersonic turbulent jet," *Physics of Fluids*, Vol. 14, No. 12, 2002, pp. 3593-3600.

[30]Ryu, J., Lele, S.K. and Viswanathan, K., "Investigation of instability waves in high-speed turbulent jets," *AIAA paper*, 2007-3624.

[31]Varnier, J. and Gély, D., "Caractérisation aérodynamique et acoustique d'un jet fortement supersonique en présence d'un obstacle plan," RT 112/3643, 1998.

[32]Lele, S.K., "Compact finite difference schemes with spectral-like resolution," *J. Comput. Phys.*, Vol. 103, 1992, pp. 16-42.

[33]Tam, C. and Webb, J., "Dispersion-relation-preserving finite difference schemes for computational aeroacoustics," *J. Comput. Phys.*, Vol. 107, No. 2, 1993, pp. 262-281.

[34]Bogey, C. and Bailly, C., "A family of low dispersive and low dissipative explicit schemes for flow and noise computations," *J. Comput. Phys.*, Vol. 194, No. 1, 2004, pp. 194-214.

[35]Bogey, C., de Cacqueray, N. and Bailly, C., "A shock capturing methodology based on adaptative spatial filtering for high-order non-linear computations," *J. Comput. Phys.*, Vol. 228, No. 5, 2009, pp. 1447-1465.

[36]Bogey, C. and Bailly, C., "Computation of high Reynolds number jet and its radiated noise using large eddy simulation based on explicit filtering," *Computer and Fluids*, Vol. 35, No. 10, 2006, pp. 1344-1358.

[37]Bogey, C. and Bailly, C. "Turbulence and energy budget in a self-preserving round jet: direct evaluation using large-eddy simulation," *Journal of Fluid Mechanics*, Vol. 627, 2009, pp. 129-160.

[38]Bodony, D.J. and Lele S.K., "Current status of jet noise predictions using large-eddy simulation," *AIAA Journal*, Vol. 46, No. 2, 2008.

[39]Liu, J.L., Ramamurti, R., Munday, D., Gutmark, E. and Lohoner, R., "Large-eddy simulations of a supersonic jet and its near-field acoustic properties," *AIAA Journal*, Vol. 47, No. 8, 2009, pp. 1849-1863.

[40]Mendez, S., Shoeybi, M., Sharma, A., Ham, F.E., Lele, S.K. and Moin, P., "Large-eddy simulations of perfectly-expanded supersonic jets: quality assessment and validation", *AIAA-2010-271*, 2010.

[41]Berland, J.,Bogey, C., Marsden, O. and Bailly, C., "High-order, low dispersive and low dissipative explicit schemes for multi-scale and boundary problems," *J. Comput. Phys.*, Vol. 224, No. 2, 2007, pp. 637-662.

[42]Mohseni, K. and Colonius, T., "Numerical treatment of polar coordonate singularities," *J. Comput. Phys.*, Vol. 157, 2000, pp. 787-795.

[43]Bogey, C., de Cacqueray, N. and Bailly, C., "Finite differences for coarse azimuthal discretization and for reduction of effective resolution near origin of cylindrical flow equations," *submitted to J. Comput. Phys.*.

[44]Bogey, C. and Bailly, C. "Three-dimensional non-reflective boundary conditions for acoustic simulations: far field formulation and validation test cases," *Acta Acustica United with Acustica*, Vol. 8, 2002, pp. 463-471.

[45]Bogey, C. and Bailly, C., "Large Eddy Simulations of transitional round jets: influence of the Reynolds number on flow development and energy dissipation," *Physics of Fluids*, Vol. 18, No. 6, 2006, pp. 1-14.

[46]Hornung, H. and Schwendeman, D., "Oblique shock reflection from an axis of symmetry: shock dynamics and relation to the Guderley singularity," *Journal of Fluid Mechanics*, Vol. 438, 2001, pp. 231-245.

[47]Hussein, H.J., Capp, S.P. and George, W.K., "Velocity measurement in a high-Reynolds-number, momentum-concerving, axisymmetric, turbulente jet," *Journal Fluid Mechanics*, Vol. 258, 1994, pp. 31-75.

[48]Norum, T.D. and Seiner, J.M., "Measurements of mean static pressure and far-field acoustics of shock-containing supersonic jets," *NASA TM-84521*, 1982.

[49]Tam, C.K.W., and Tanna, H.K., "Shock associated noise of supersonic jets from convergent-divergent nozzles," *Journal of Sound and Vibration*, Vol. 81, No. 3, 1982, pp. 337-357.

[50]Morris, P.J., Bhat, T.R.S. and Chen, C., "A linear shock cell model for jets of arbitrary exit geometry," *Journal of Sound of Vibration*, Vol. 132, No. 2, 1989, pp. 199-211.

[51]Freund J.B., Lele, S.K. and Moin, P., "Compressible effects in a turbulent annular mixing layer. Part 1. Turbulence and growth rate," *Journal of Fluid Mechanics*, Vol. 421, 2000, pp. 229-267.

[52]Troutt, T.R. and McLaughlin, D.K., "Experiments on the flow and acoustic properties of moderate-Reynolds-number supersonic jet," *Journal of Fluid Mechanics*, Vol. 116, 1982, pp. 123-156.

[53]Papamoschou, D., Morris, P.J. and Mclaughlin, D.K., "Beamformed flow-acoustic correlations in high-speeds jets," *AIAA Paper*, 2009-3212.

[54]Greska, B., Krothapalli, A., Horne, W. and Burnside, N., "A near-field study of high temperature supersonic jets," AIAA Paper 2008-3026, 2008.

[55]Mclaughlin, D.K., Morrison, G.L. and Troutt, T.R. "Reynolds number dependence in supersonic jet noise," *AIAA Journal*, Vol. 14, No. 4, 1977, pp. 526-532.

[56]Zaman, K.B.M.Q., "Effect of initial condition on subsonic jet noise," *AIAA Journal*, Vol. 23, No. 9, 1985.

[57]Bogey, C. and Bailly, C., "Influence of nozzle-exit boundary layer conditions on the flow and acoustic fields of initially laminar jets," *submitted to J. Fluid Mech.*, 2010.

[58]Bodony, D.J., Ryu, J. and Lele, S.K., "Investigating broadband shock-associated noise of axisymmetric jets using large-eddy simulation," *AIAA Paper*, 2006-2495.

[59]Ponton, M.K. and Seiner, J.M., "The effects of nozzle lip thickness on plume resonance," *Journal of Sound and Vibration*, Vol. 154, No. 3, 1992, pp. 531-549.

[60]Juve, D., Sunyach, M. and Comte-Bellot, G., "Filtered azimuthal correlations in the acoustic far-field of a subsonic jet," *AIAA Journal*, Vol. 17, No. 1, 1979, pp. 112-114.